NONLINEAR ANALYSIS OF REINFORCED CONCRETE STRUCTURES USING QUADRILATERAL MEMBRANE ELEMENTS

Ole Strøm, Dr.ing., A/S Veritec, Høvik, Norway

Four noded membrane element, that include concrete and reinforcement, has been developed. Large rotations and displacements can be handled. Green strains and second Piola-Kirchhoff stresses are used.

Cracking, crushing, creep and shear retention during cracking are some of the effects that are included in the concrete model. Different properties in tension and compression, and closing and reopening of cracks are features of the programe.

Keywords: FEM, nonlinear, concrete, creep

1. GENERAL

This paper deals with nonlinear finite element analyses of reinforced concrete plates loaded in their own plane. Four noded membrane element, that include concrete and up to two types of reinforcement, has been developed. This composite element is quite efficient and can be used for situations involving large rotations, displacements and instabilities. The element, which may be of plane stress or plane strain, may be arbitrary oriented in three-dimensional space.

Conservative, non-conservative and cyclic loadings can be applied. An updated description of motion for large displacement analysis is used. This theory is simplified for small strains, however, large rotation effects are allowed for. Green strains and second Piola-Kirchhoff stresses are used. Coordinate systems for the updated formulation are defined. The principle of virtual work is used for establishing the fundamental equations for total and incremental equilibrium.

Cracking, crushing, creep and shear retention during cracking are some of the effects that are included in the concrete model presented here. The elastic-plastic flow theory is combined with the load surface theory of Chen and Chen. This theory allows for different properties in tension and compression. Hardening, but not softening, is included. Smeared cracking with two independent crack directions may be introduced when cracking. The constitutive equations are modified for tension cracking including closing and reopening of the cracks. A new failure criterion based on strains is included. Aggregate interlocking effects and dowel action may be included by introducing state dependent shear retention factors. The creep strains are calculated by the rate of creep method based on total strains. The numerical results are compared with the experimental results of Burns and Siess.

The mathematical model which describes the behaviour of reinforcement steel is based on the flow theory of plasticity with isotropic hardening.

This work is a part of the development of a general purpose nonlinear programme package named FENRIS. The name FENRIS is abbreviation for Finite Element NonlineaR Integrated System. This has been a joint project between the Division of Structural Mechanics at The Norwegian Institute of Technology, The Foundation for Scientific and Industrial Research at The Norwegian Institute of Technology (SINTEF) and Det norske Veritas.

2. THE COMPOSITE MEMBRANE ELEMENT

There may be up to three different materials in this element; concrete and two different layers of reinforcement. The total expressions for the internal forces and the global stiffness matrix are found by summation of the contributions from the different materials /6/.

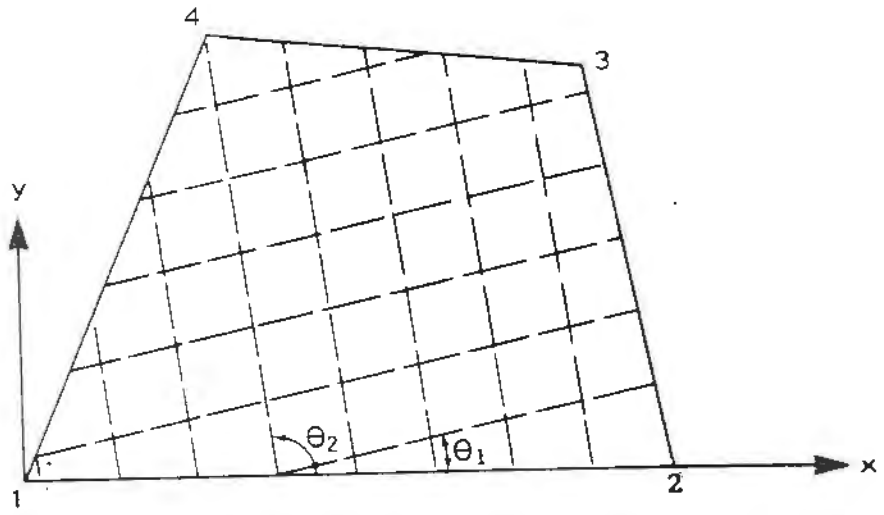

Figure 1 Reinforcement bars implemented in a membrane element.

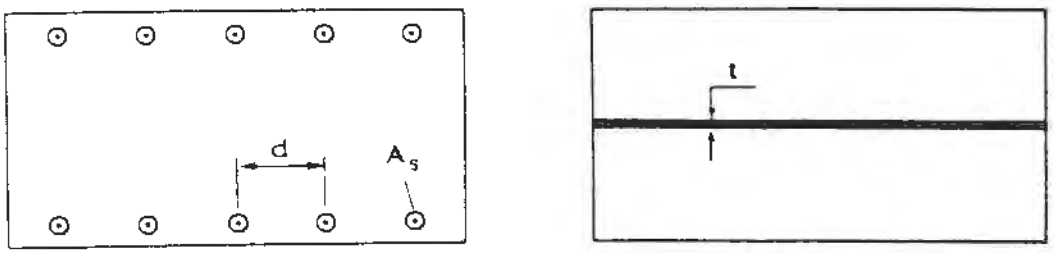

Figure 2 Idealization of the reinforcement bars.

Fig. 1 shows the modelling of the reinforcement hars. θ_1 and θ_2 are the angles between the x-axis and the reinforcement types 1 and 2, respectively. The reinforcement types 1 and 2 have only material stiffness in the directions θ_1 and θ_2, respectively, and a transformation to the x-y system has to be carried out /6/. 2x2 points Gauss integration is used over the plate area.

The reinforcement bars are "smeared out" as a continuous plate, see Fig. 2. The thickness of the equivalent reinforcement layer is /6/

$$t = \frac{n\ A_s}{d} \tag{1}$$

in which A_s is the cross-sectional area of one bar, d is the width between the bars and n is the number of reinforcement layers with exactly same material properties and direction (equal to 2 in Fig. 2). The eccentricities of the reinforcement layers in relation to the midspan of the membrane are not considered.

3. THE GENERAL THEORY OF PLASTICITY

The general flow theory /7/ assumes that the incremental strain, $\Delta\varepsilon_{ij}$, may be decomposed into a recoverable elastic part, $\Delta\varepsilon^e_{ij}$, and an irrecoverable plastic part $\Delta\varepsilon^p_{ij}$

$$\Delta\varepsilon_{ij} = \Delta\varepsilon^e_{ij} + \Delta\varepsilon^p_{ij} \tag{2}$$

It is important to note that Green strains in fact do not follow such an additive decomposition, and that the assumption of (2) is valid only for small strains. This is, however, a realistic assumption for concrete. Having this limitation in mind, the previous symbols for strains is used in the following derivations. It is assumed that the elastic strains are related to the stresses through Hooke's law. The relations between the plastic strains and the stresses depend on the chosen flow function. The flow rule is here assumed to be associated, i.e. the plastic potential surface has the same shape as the current yield or loading surface.

The plastic strain are found in many text books /7/ and is accepted here as :

$$d\varepsilon^p_{ij} = \frac{\frac{\partial f}{\partial \sigma_{rs}}\ C^e_{rskl}\ d\varepsilon_{kl}}{\left[\ h + \frac{\partial f}{\partial \sigma_{mn}}\ C^e_{mnpq}\ \frac{\partial f}{\partial \sigma_{pq}}\ \right]}\ \frac{\partial f}{\partial \sigma_{ij}} \tag{3}$$

where $\frac{\partial f}{\partial \sigma_{rs}}$ is the derivated of the load function with respect to the stresses, C^e_{rskl} is the elastic constitutive matrix and h is a hardening parameter.

The stress-strain relation of an elastic-workhardening-plastic solid is then obtained by substitution of equation (3) into the expression for the stress increment :

$$d\sigma_{ij} = C^e_{ijkl}\ d\varepsilon^e_{kl} = C^e_{ijkl}\ (d\varepsilon_{kl} - d\varepsilon^p_{kl}) \tag{4}$$

which can be rewritten to :

$$d\sigma_{ij} = C^{ep}_{ijkl}\ d\varepsilon_{kl} = (C^e_{ijkl} + C^p_{ijkl})\ d\varepsilon_{kl} \tag{5}$$

where C^{ep}_{ijkl} is the elastic-plastic constitutive matrix, and where the plastic constitutive matrix, C^p_{ijkl}, has the form

$$C^p_{ijkl} = -\frac{C^e_{ijtu}\ \frac{\partial f}{\partial \sigma_{rs}}\ \frac{\partial f}{\partial \sigma_{tu}}\ C^e_{rskl}}{\left[\ h + \frac{\partial f}{\partial \sigma_{mn}}\ C^e_{mnpq}\ \frac{\partial f}{\partial \sigma_{pq}}\ \right]} \tag{6}$$

4. THE FLOW THEORY BY CHEN AND CHEN

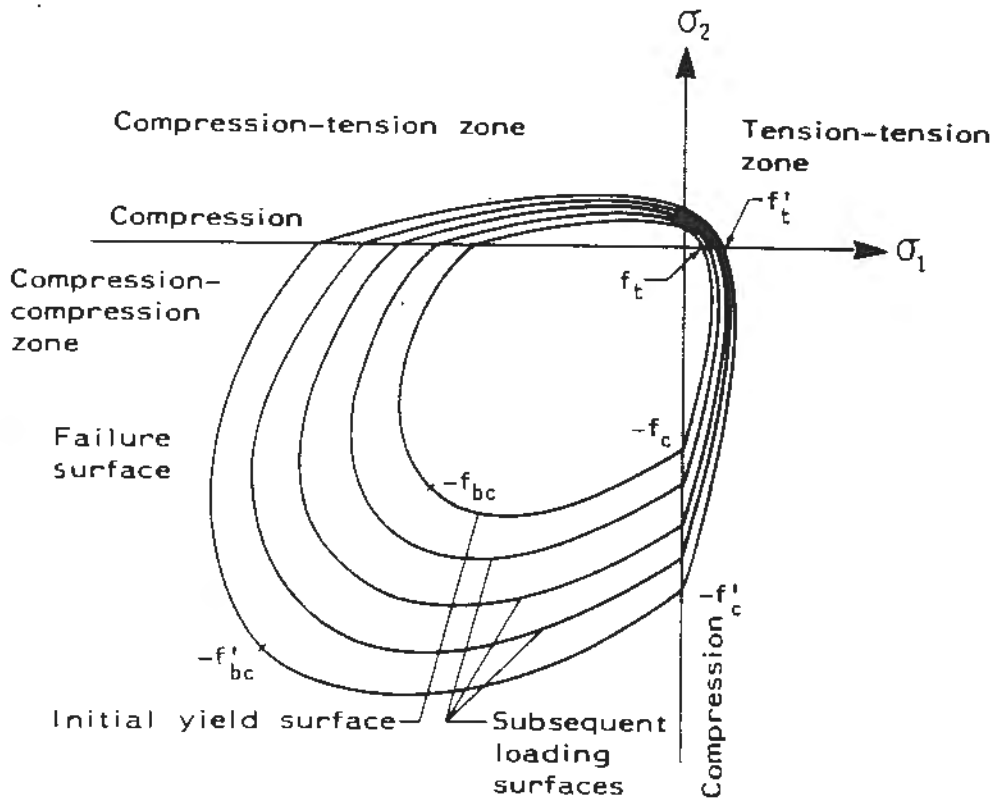

Figure 3 Loading surfaces of concrete in the biaxial stress plane.

Chen and Chen postulated an initial, non-smooth yield surface with subsequent loading surfaces, and a failure surface for concrete. These surfaces in two-dimensional principal stress space are traced in Fig. 3. The concrete is treated as an elastic-plastic strain hardening material with fracturing behaviour in tension.

Three mathematical equations are used to define Chen and Chen's loading surfaces /3,4/

1) An initial discontinuous loading surface

$$f_o = \sqrt{\frac{\kappa^2}{3} J_2^\sigma - \frac{\kappa^2}{36} (I_1^\sigma)^2 \pm \frac{1}{12}(I_1^\sigma)^2 + \frac{A_o}{3} I_1^\sigma} - \tau_o \tag{7}$$

2) Subsequent loading surfaces

$$f = \frac{\sqrt{\frac{\kappa^2}{3} J_2^\sigma - \frac{\kappa^2}{36} (I_1^\sigma)^2 \pm \frac{1}{12}(I_1^\sigma)^2 + \frac{\beta}{3} I_1^\sigma}}{\sqrt{1 - \frac{\alpha}{3} I_1^\sigma}} - \tau \tag{8}$$

3) An ultimate failure loading surface

$$f_u = \sqrt{\frac{\kappa^2}{3} J_2^\sigma - \frac{\kappa^2}{36} (I_1^\sigma)^2 \pm \frac{1}{12}(I_1^\sigma)^2 + \frac{A_u}{3} I_1^\sigma} - \tau_u \tag{9}$$

The material constants, A_o, τ_o, A_u and τ_u are functions of the material parameters f_c, f'_c, f_t, f'_t, f_{bc} and f'_{bc}. Here, f'_c, f'_t and f'_{bc} denote the ultimate strength of concrete under uniaxial compressive loading, uniaxial tensile loading, and equal biaxial compressive loading, respectively, while f_c, f_t and f_{bc} denote the initial yield strength of concrete under uniaxial compressive loading, uniaxial tensile loading and equal biaxial compressive loading. These

parameters are also illustrated in Fig. 3. The value of κ^2 has been discussed very extensively in refs. /3,4/, and it is set equal to 3.0 in this work. The positive-negative sign in the third term in Eqs. (7) to (9) represents the loading function in the "compression-compression zone" and the "tension-compression and tension-tension zone", respectively.

The loading surfaces, which are functions of the history of loading, are derived from an isotropic expansion of the initial yield surface, until coincidence with the failure surface f_u is reached. The failure surface f_u is the outmost extreme loading surface. Since the loading surface shall coincide with the initial yield surface and the failure surface as extreme cases, the constants α and β will be

$$\alpha = \frac{A_u - A_o}{\tau_u^2 - \tau_o^2} \qquad \beta = \frac{A_o\,\tau_u^2 - A_u\,\tau_o^2}{\tau_u^2 - \tau_o^2} \tag{10}$$

The flow function given by equation (8) may be used in the equation (6). For the case of plane stress ($\sigma_{zz} = \sigma_{xz} = \sigma_{yz} = 0$) equation (5) /3/ will be

$$\begin{Vmatrix} d\sigma_{xx} \\ d\sigma_{yy} \\ d\sigma_{xy} \end{Vmatrix} = \frac{E_o}{(1-\nu^2)} \begin{vmatrix} 1-\omega\Phi_{11} & \nu-\omega\Phi_{12} & -\omega\Phi_{13} \\ & 1-\omega\Phi_{22} & -\omega\Phi_{23} \\ & & \frac{(1-\nu)}{2}-\Phi_{33} \end{vmatrix} \begin{Vmatrix} d\varepsilon_{xx} \\ d\varepsilon_{yy} \\ 2d\varepsilon_{xy} \end{Vmatrix} \tag{11}$$

in which

$$\frac{1}{\omega} = 2(1-\nu)J_2^{\sigma} - (1-2\nu)\sigma_{zz}'^2 - 2(1+\nu)\rho\sigma_{zz}' + 2(1+\nu)\rho^2 + (1 - \frac{\alpha I_1^{\sigma}}{3})\frac{H(1-\nu^2)}{E_o}\sqrt{2J_2^{\sigma} + 2\rho^2} \tag{12}$$

$$\Phi_{11} = [(1-\nu)\sigma_{xx}' - \nu\sigma_{zz}' + (1+\nu)\rho]^2 \tag{13}$$

$$\Phi_{12} = [(1-\nu)\sigma_{xx}' - \nu\sigma_{zz}' + (1+\nu)\rho]\,[(1-\nu)\sigma_{yy}' - \nu\sigma_{zz}' + (1+\nu)\rho] \tag{14}$$

$$\Phi_{13} = [(1-\nu)\sigma_{xx}' - \nu\sigma_{zz}' + (1+\nu)\rho]\,[(1-\nu)\sigma_{xy}] \tag{15}$$

$$\Phi_{22} = [(1-\nu)\sigma_{yy}' - \nu\sigma_{zz}' + (1+\nu)\rho]^2 \tag{16}$$

$$\Phi_{23} = [(1-\nu)\sigma_{yy}' - \nu\sigma_{zz}' + (1+\nu)\rho]\,[(1-\nu)\sigma_{xy}] \tag{17}$$

$$\Phi_{33} = [(1-\nu)\sigma_{xy}]^2 \tag{18}$$

where ε_o is the initial modulus of elasticity, H is a strain-hardening rate function and ν is Poisson's ratio. Further we have that σ_{xx}', σ_{yy}', σ_{zz}' are the deviatoric stress components, I_1^{σ} is the first invariant of the total stresses and J_2^{σ} is the second invariant of the deviatoric stresses. ρ is given by equation (19)

$$\rho = \frac{(\pm 3 - \kappa^2)}{18} I_1^{\sigma} + \frac{(\beta + \alpha\tau^2)}{3} \tag{19}$$

The strain-rate function, H, depends upon the current state of stress, strain and straining history. H may be written as :

$$H = (\frac{2}{3})^{1.5} |\bar{\sigma}_{xx}| \frac{E_o E_t}{(E_o - E_t)} \tag{20}$$

where $\bar{\sigma}_{xx}$ is the one-dimensional compressive stress corresponding to the total equivalent plastic strain, which is given hy

$$\bar{\varepsilon}_p = \int d\bar{\varepsilon}^p = \int \sqrt{\frac{2}{3} d\varepsilon_{ij}^p d\varepsilon_{ij}^p} \tag{21}$$

Since $\bar{\varepsilon}^p$ and $\bar{\sigma}_{xx}$ always are related to the compression part of the one-dimensional stress-strain curve, the tangent stiffness, E_t, will also always be from the compression branch of the one-dimensional stress-strain curve. It may be a weakness that E_t is calculated from the compression part of the one-dimensional stress-strain curve regardless of the signs of the biaxial stresses. However, this is not a bad assumption since the strain-cracking criteria in the tension-compression zone and the tension-tension zone, see Eq. (29) and (30), leads to material failure at maximum allowed tension strains.

5. TENSION CRACKING AND CRUSHING OF CONCRETE

Tension cracking of concrete in the membrane elements may happen in two independent directions per integration point. For these elements the cracks are always formed normal to the element plane.

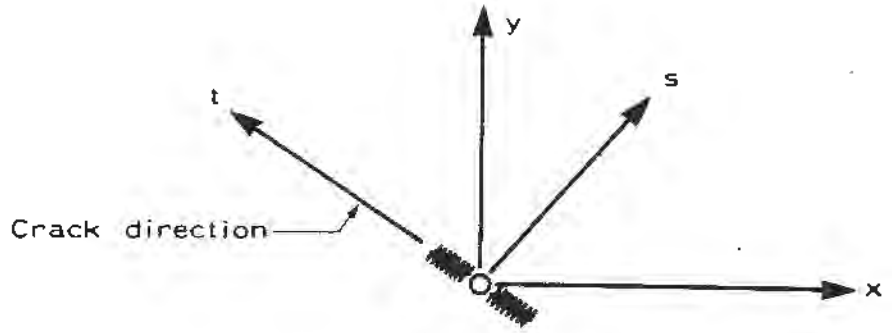

Figure 4 Local coordinate system for a crack.

The current stresses are used to find the principal stresses, σ_{st}, and their directions s and t, see Fig. 4. The strains for the same direction, ε_{st}, are also calculated.

The tangential constitutive matrix of the integration point for the uncracked concrete is also transformed to the direction of the principal stresses. The incremental stress-strain relation will then be

$$\begin{vmatrix} \Delta\sigma_{ss} \\ \Delta\sigma_{tt} \\ \Delta\sigma_{st} \end{vmatrix} = \begin{vmatrix} C_{11} & C_{12} & C_{13} \\ C_{21} & C_{22} & C_{23} \\ C_{31} & C_{32} & C_{33} \end{vmatrix}_{st}^{ep} \begin{vmatrix} \Delta\varepsilon_{ss} \\ \Delta\varepsilon_{tt} \\ 2\Delta\varepsilon_{st} \end{vmatrix} \tag{22}$$

or

$$\Delta\sigma_{st} = \mathbf{C}_{st}^{ep}\Delta\varepsilon_{st} \tag{23}$$

If the stress point is outside the failure surface in the tension-compression zone or in the tension-tension zone a crack is formed in the plane of the membrane normal to the greatest principal stress. The direction of this crack will be stored and unaltered through the further calculations. And this crack will influence the local stiffness matrix as long as the strain normal to the crack is greater than zero. If later the second principal stress becomes greater than f_t' an additional crack is formed. The direction of the second crack is not necessary normal to the first crack. Also the second crack direction will be stored and unaltered through the further calculations. The second crack will only influence the local stiffness

matrix as long as the strain normal to the crack is greater than zero.

Alternatively cracks can also be formed if the strain criterion (30) is exceeded. After cracking $\mathbf{C}_{xy}^{ep}$ and $\mathbf{C}_{st}^{ep}$ is taken to be modified matrices from the initial linear elastic matrix. The stress normal to the crack drops to zero, which implies

$$\sigma_{ss} = \Delta\sigma_{ss} = 0 \tag{24}$$

The first row of Eq. (22), when $C_{13}=C_{23}=C_{31}=C_{32}=0$, gives

$$\Delta\varepsilon_{ss} = -\frac{C_{12}}{C_{11}}\Delta\varepsilon_{tt} \tag{25}$$

Substituting Eq. (25) into the second row of Eq. (22) the modified constitutive relation for a cracked integration point becomes

$$\begin{Bmatrix} \Delta\sigma_{ss} \\ \Delta\sigma_{tt} \\ \Delta\sigma_{st} \end{Bmatrix} = \begin{bmatrix} 0 & 0 & 0 \\ 0 & (C_{22}-\frac{C_{12}C_{21}}{C_{11}}) & 0 \\ 0 & 0 & \beta C_{33} \end{bmatrix}_{st}^{e} \begin{Bmatrix} \Delta\varepsilon_{ss} \\ \Delta\varepsilon_{tt} \\ 2\Delta\varepsilon_{st} \end{Bmatrix} \tag{26}$$

or

$$\Delta\sigma_{st} = \mathbf{C}_{st}^{e}\Delta\varepsilon_{st} \tag{27}$$

The shear retention factor, β, takes care of the retained shear stiffness when cracking. This factor retains some shear stiffness for sliding movement parallel to the crack, aggregate interlocking and dowel action /8/. β has to be between zero (no shear) and one (no shear reduction). Many values of β have been proposed, i.e. from different constants to linear, bilinear and nonlinear curves as functions of the strain normal to the crack. When β is set equal to zero the occurrance of the second crack is limited to occur orthogonally to the first crack, and it may therefore violate the tension failure criterion within the element. As long as β is greater than zero for singly cracked concrete the direction of the principal concrete stress allows to rotate, and subsequent cracking to occur in new directions non-orthogonal to the initial crack direction. Models which retain some shear stiffness after the first crack, but do not reorientate the material axis after formation of the second crack, require orthogonal cracking to obtain zero normal stress on both crack faces. In this case β is set equal to zero (no tension stiffening) after the second crack.

If two cracks are formed both normal stresses drop to zero and the stiffness matrix in the direction of the first crack is

$$\mathbf{C}_{st}^{e} = \begin{bmatrix} 0 & 0 & 0 \\ 0 & 0 & 0 \\ 0 & 0 & \beta C_{33} \end{bmatrix}_{st}^{e} \tag{28}$$

If one of the cracks is closed the stiffness matrix $\mathbf{C}_{st}^{e}$ will be as for one crack. If both cracks close the stiffness matrix $\mathbf{C}_{st}^{e}$ will be as for a virgin material.

The theory of A.C.T.Chen and W.F.Chen /7/ also includes a failure criterion based on strains, this is illustrated in Fig. 5. The strain criterion is :

$$f'(\varepsilon_{ij}) = J_2^{\varepsilon} + \frac{A_u}{3}\frac{\varepsilon_c'}{f_c'} I_1^{\varepsilon} = \tau_u^2 \left(\frac{\varepsilon_c'}{f_c'}\right)^2 \tag{29}$$

or

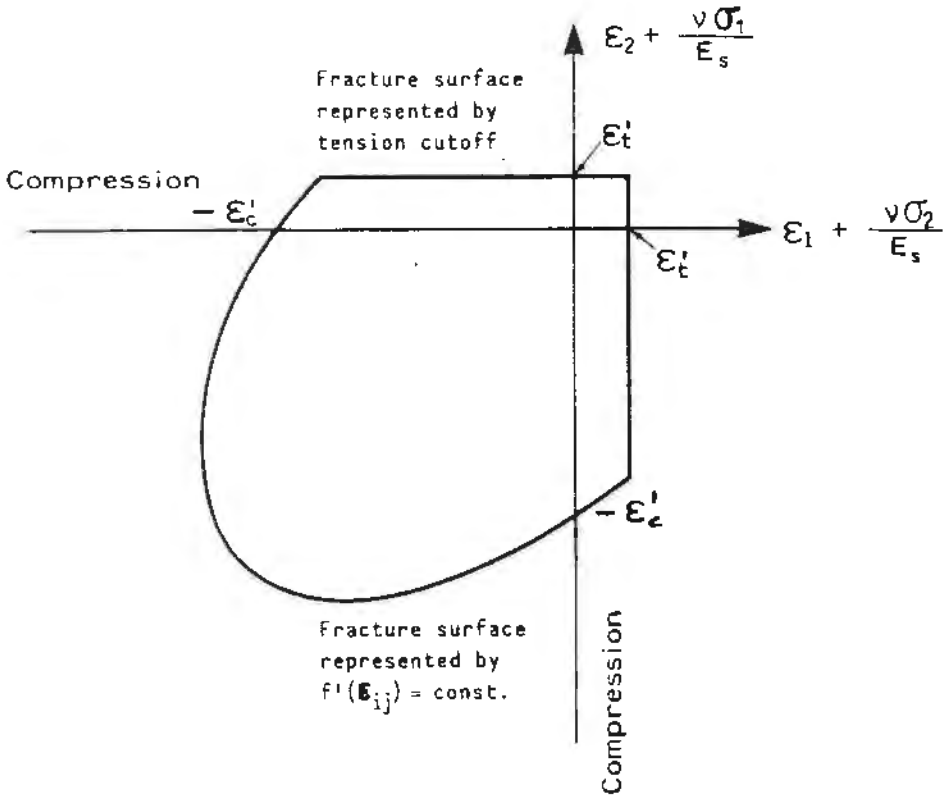

Figure 5 Fracture surface defined by strain components in the biaxial strain plane.

$$\varepsilon_1 = \varepsilon_t' - \frac{\nu\sigma_2}{E_s} \quad , \quad \varepsilon_2 = \varepsilon_t' - \frac{\nu\sigma_1}{E_s} \tag{30}$$

where I_1^ε is the first invariant of the toal strains, and J_2^ε is the second invarian of the deviatoric strains. ε_1 and ε_2 are the two principle strains, while σ_1 and σ_2 are the stresses in the direction of the principle strains. E_s is the one-dimensional secant stiffness for the stresses σ_1 and σ_2.

If the stresses are so high that the current loading surface lies outside the compression-compression failure surface, then the concrete is crushed at this integration point. All stresses then remain at the ultimate level, while the stiffness matrix for the same integration point drops to a zero matrix, see equation (31). This condition will always be maintained for this integration point.

$$\mathbf{C}_{sl}^{ep} = \mathbf{0} \tag{31}$$

Before leaving the material routine the principal stresses, the strains and the tangential constitutive matrix $\mathbf{C}_{sl}^{ep}$ are transformed back to the x-y system.

6. MATHEMATICAL MODELLING OF REINFORCEMENT STEEL

The reinforcement has stiffness in only the direction of the bars. Since this direction in general will not coincide with the local coordinate directions of the element, see Fig. 1, a transformation has to be carried out. Let s and t be the direction of the bar and the direction normal to the bar, respectively. Stresses and strains are transformed from the local x,y-

system to the rotated s,t-system.

The uniaxial material law of the reinforcement layers can be expanded by including all in-plane stress and strain components. The corresponding stress-strain equation in the s-t coordinate system is

$$\begin{Bmatrix} \Delta\sigma_{ss} \\ \Delta\sigma_{tt} \\ \Delta\sigma_{st} \end{Bmatrix}^{s} = E_t \begin{bmatrix} 1 & 0 & 0 \\ 0 & 0 & 0 \\ 0 & 0 & 0 \end{bmatrix} \begin{Bmatrix} \Delta\varepsilon_{ss} \\ \Delta\varepsilon_{tt} \\ 2\Delta\varepsilon_{st} \end{Bmatrix}^{s} \tag{32}$$

where E_t is the tangent modulus of the uniaxial stress-strain relation for the reinforcing steel. Before leaving the material routine the stresses, strains and the tangential constitutive matrix are transformed back to the x-y system.

7. APPLICATION OF THE RATE OF CREEP METHOD (RCM)

The Rate of Creep Method presented here is due to Glanville /9/, and it was first applied to more complicated problems by Dischinger /10,11/. The creep strain rate is assumed to be a function of the current stresses, σ_{xy}, and the elapsed time from loading, i.e.

$$\frac{d\varepsilon_{xyc}(t-\tau)}{dt} = f(\sigma_{xy}, t-\tau) \tag{33}$$

or more specifically

$$\frac{d\varepsilon_{xyc}(t-\tau)}{dt} = \varepsilon_{xy} \frac{d\varphi(t,\tau)}{dt} \tag{34}$$

Where the creep function $\varphi(t,\tau)$ is given by the hyperbolic expression :

$$\varphi(t,\tau) = \frac{t-\tau}{t_{0.5}+t-\tau} \varphi(\infty,\tau) \tag{35}$$

in which $\varphi(\infty,\tau)$ is the limit value of $\varphi(t,\tau)$ at infinity. t is the current time from casting of concrete (in days). τ is the age at loading (in days), and $t_{0.5}$ is the time (in days) corresponding to half limit value, i.e. $\varphi(t_{0.5},\tau) = 0.5\ \varphi(\infty,\tau)$

Regardless of the stress level the creep strain can be obtained by integrating equation (34)

$$\varepsilon_{xyc}(t,\tau) = \int_{\tau}^{t} \varepsilon_{xy} \frac{d\varphi(t,\tau)}{dt}\, dt \tag{36}$$

ε_{xy} is taken as the strain without creep at the time t.

Since this programme is based on an incremental formulation the incremental creep strains are calculated as follows

$$\Delta\varepsilon_{xyc}(t,\tau) = \varepsilon_{xy} \cdot \Delta\varphi(t,\tau) = \varepsilon_{xy} \cdot (\varphi(t+\Delta t,\tau) - \varphi(t,\tau)) \tag{37}$$

where t is the time at the beginning of the time increment Δt. And when the creep factor in equation (34) is used

$$\Delta\varepsilon_{xyc}(t,\tau) = \varepsilon_{xy} \cdot \left\{\frac{t+\Delta t-\tau}{t_{0.5}+t+\Delta t-\tau} - \frac{t-\tau}{t_{0.5}+t-\tau}\right\} \cdot \varphi(\infty,\tau) \tag{38}$$

In general the accuracy increases with decreasing size of the time increments; therefore, a relatively large number of time steps should be used for problems with high stresses and long duration. Fixed time increments may be given as input to the programme. However, if the time steps give $\Delta\varphi(t,\tau)$ greater than 10% of $\varphi(\infty,\tau)$ the current time step is automatically

reduced. And so $\Delta\varphi(t,\tau)$ will never be greater than 0.1 $\varphi(\infty,\tau)$.

It should be mentioned that the rate of creep method does not consider the strain history; therefore, creep recovery is not described. Only the current stresses are considered. The method disregards the stress history in the calculation of the next increment (the rate equation does not account for the history). Note, however, that the incremental creep strains are accumulated step by step, thus, the total creep strains will then depend on the history. The method is not suited for load reversals.

8. NUMERICAL STUDIES

EXAMPLE 1: Cyclic Loading of a Simply Supported Beam.

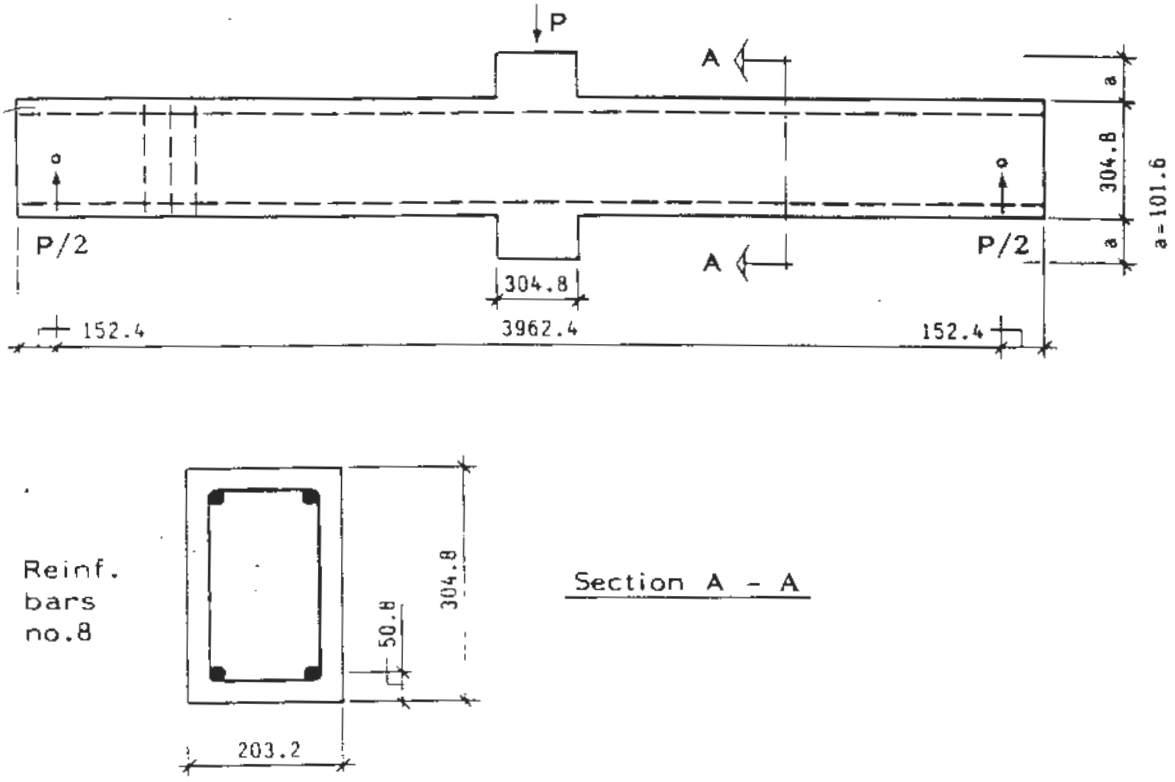

Figure 6 Beam J-3 tested by Burns and Siess. All measures in mm.

The simply supported reinforced concrete beam shown in Fig. 6 has been tested experimentally during cyclic loading by Burns and Siess /12/. This beam has been investigated by the theories described earlier in this paper. Due to symmetry only one half of the beam has been analysed. A 6 by 6 mesh is used, see Fig. 7. The longitudinal reinforcement bars are indicated by the dashed lines, and this reinforcement is "smeared out" in the two lowest and the two highest rows of elements in such a way that the moment of inertia is the same. The stirrups have been neglected in the computational model. The beam is modelled with constant height all over the length.

Fig. 8 shows the material properties for the concrete. No experimental value of the initial modulus of elasticity, E_o, was given by Burns and Siess /12/, and therefore E_o was chosen

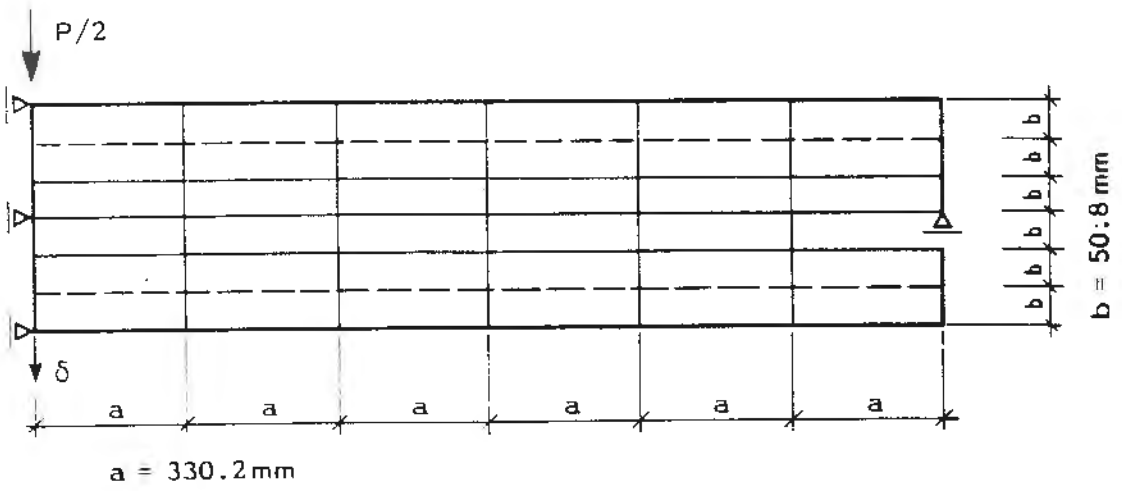

Figure 7 Finite element model of half the beam.

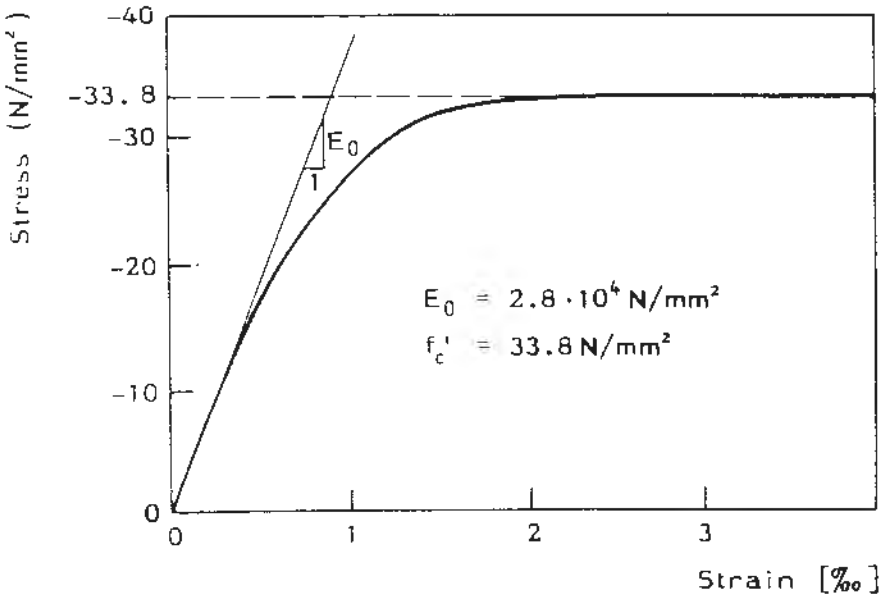

Figure 8 Uniaxial stress-strain curve for concrete.

such that it gave the same load-deflection curve as the experimental curve for P up to 10kN. The cracking strain, ε_t', was assumed so that initial cracking occurred at the load level reported in ref. /12/. In tension the concrete was modeled by a bilinear curve (with $\varepsilon_t = 0.075 \cdot 10^{-3}, f_t = 2.175 \text{N/mm}^2, \varepsilon_t' = 0.125 \cdot 10^{-3}, f_t' = 3.623 \text{N/mm}^2$. Poisson's ratio, ν, was set to 0.18, and the shear retention factor, β, was set to 1.0. Cracking was tested for at every iteration.

Mild steel bars with typical yield level in monotonic loading were used in the experimental test. The reinforcement is modeled by elastic-plastic flow theory with isotropic hardening. The

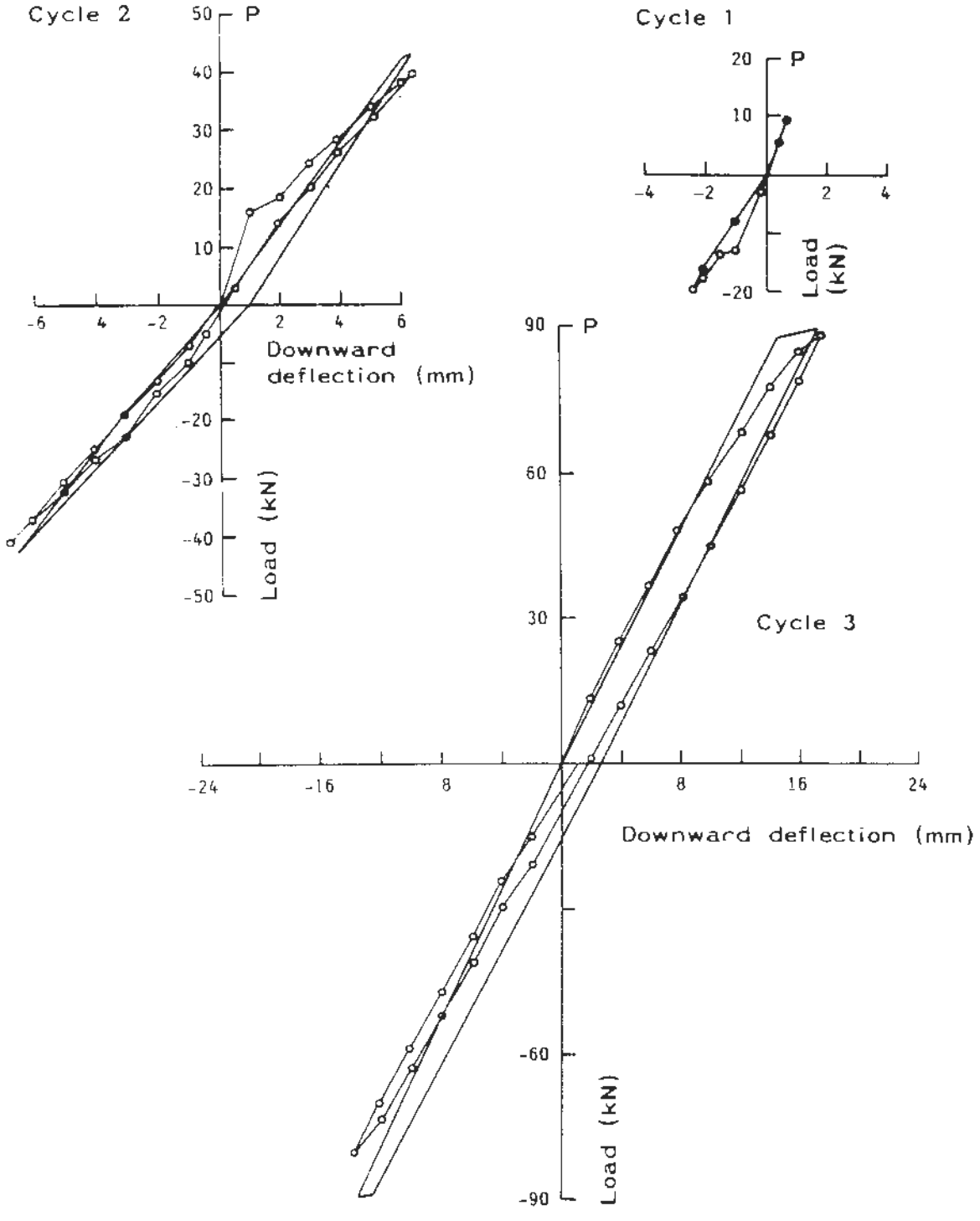

Figure 9 a Deflection cycling of the simply supported beam. The cycles 1, 2 and 3.

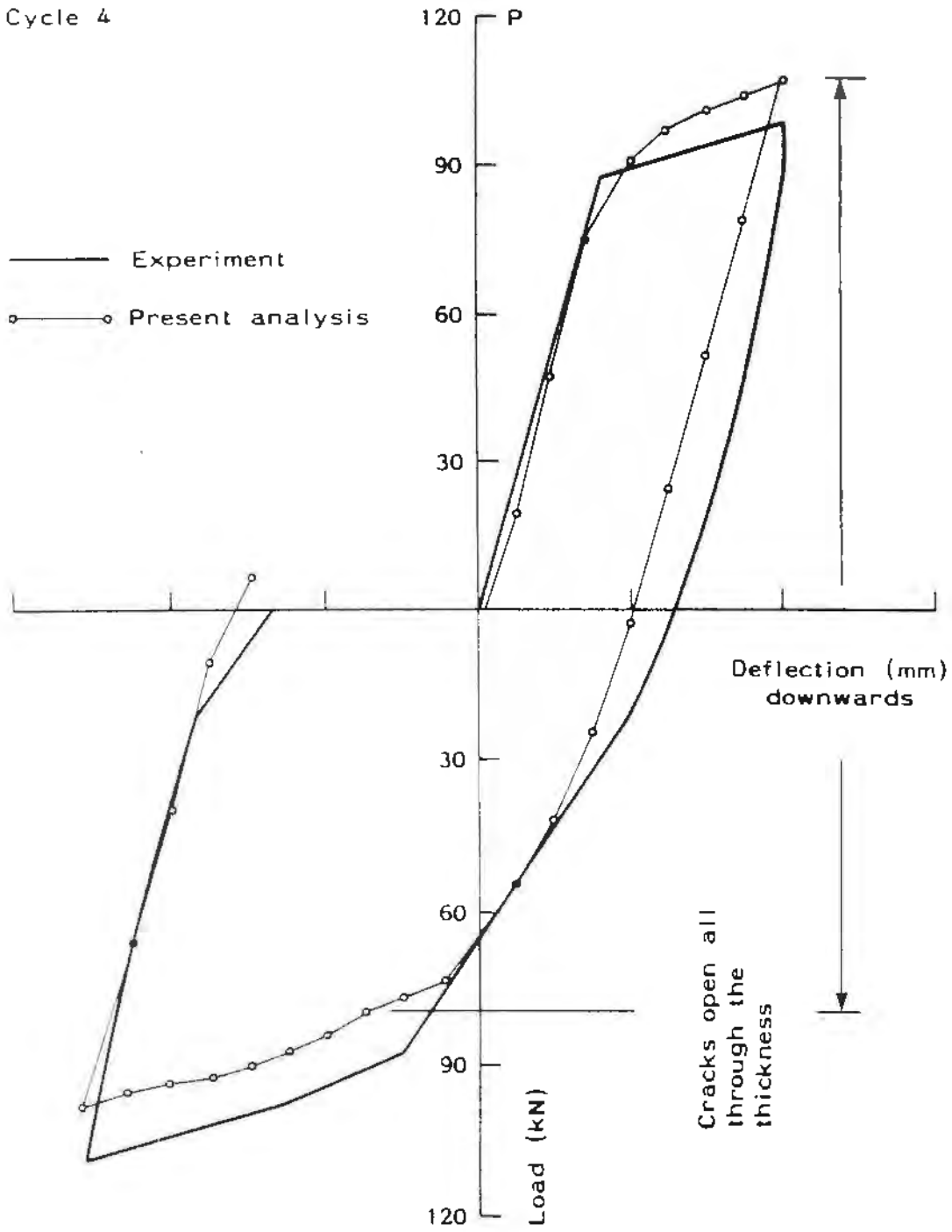

Figure 9 b Deflection cycling of the simply supported beam. The cycle 4.

EXAMPLE 2 : Creep Deformations of a Hinged Column.

One of the most comprehensive, large scale experimental creep investigation of columns was done by Goyal and Jackson /14/. 26 out of a series of 46 columns were subjected to short-time loading, whereas sustained loading was applied to the remaining 20 columns. These 20 columns, one of them shown in Fig. 10, were loaded approximately 28 days after casting up to 60 per cent of the corresponding maximum short-time load. This load was remained 180 days.

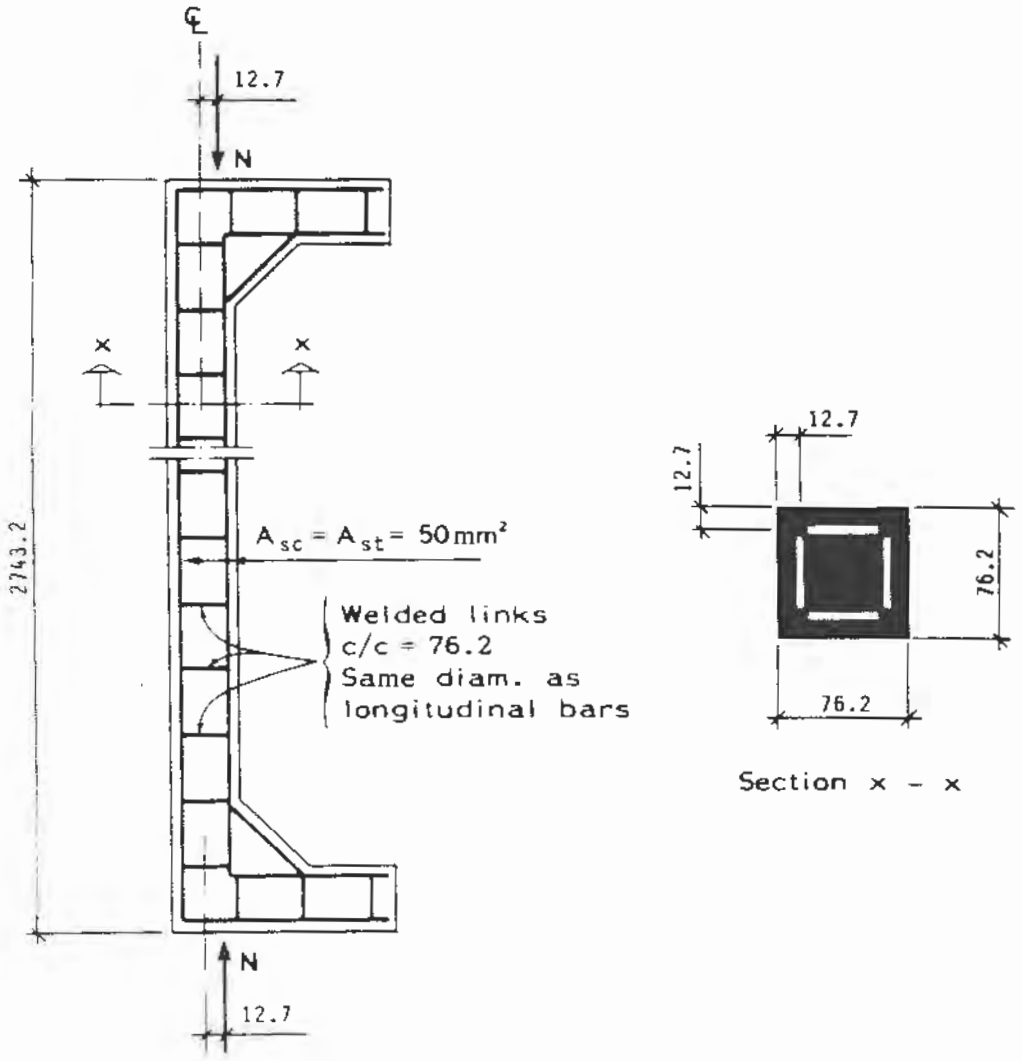

Figure 10 Geometry and reinforcement of column. All measures in mm.

The geometry of the investigated column is shown in Fig. 10. Note that the reinforcement of the column itself is symmetric. Again the effect of the stirrups has been neglected. The reinforcement bars are indicated by the dashed lines in Fig. 11, and this reinforcement is "smeared out" in the two lowest and the two highest rows of elements in such a way that the moment of inertia is the same. 36 elements were used to model half the column. The eccentric load in Fig. 10 was replaced with a load and a moment around the center line of the height.

The assumed stress-strain curve for concrete in compression is shown in Fig. 12. Unfortunately the material data given in ref. /14/ were incomplete. Complete stress-strain curves

for the test cylinders were not reported in ref. /14/. Therefore the stress-strain curves used by Åldstedt /15/ were also used here. The concrete properties in tension were neglected, see ref. /15/. Cracking was tested for at every iteration. Poisson's ratio, ν, was set to 0.18. The shear retention factor, β, was set to 1.0. Cracking was tested for at every iteration.

The steel was modelled linear elastic to the strain $1.551 \cdot 10^{-3}$ and the stress 316.4N/mm^2. Behind this point the tangential stiffness was nearly zero.

The global stiffness matrix was updated for every iteration at each load step. The convergence criterion was set to $0.1 \cdot 10^{-3}$. The convergence rate was quite low.

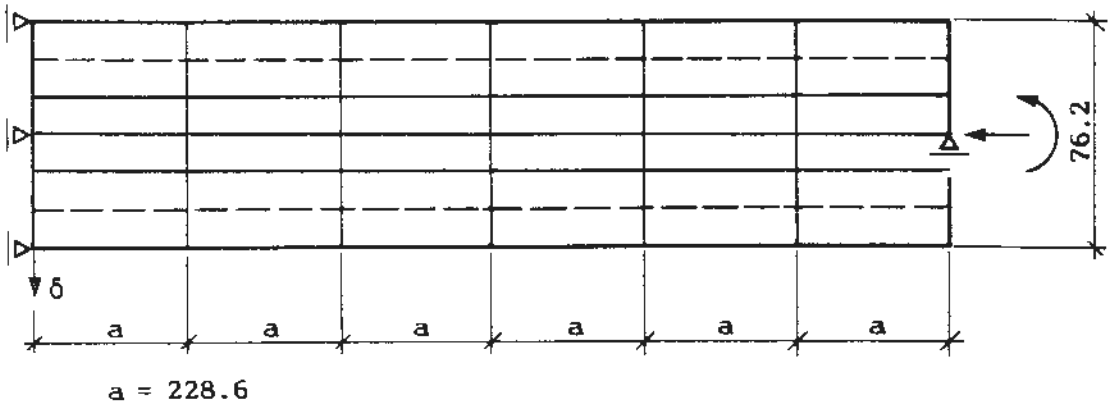

Figure 11 Finite element model of half the column. All measures in mm.

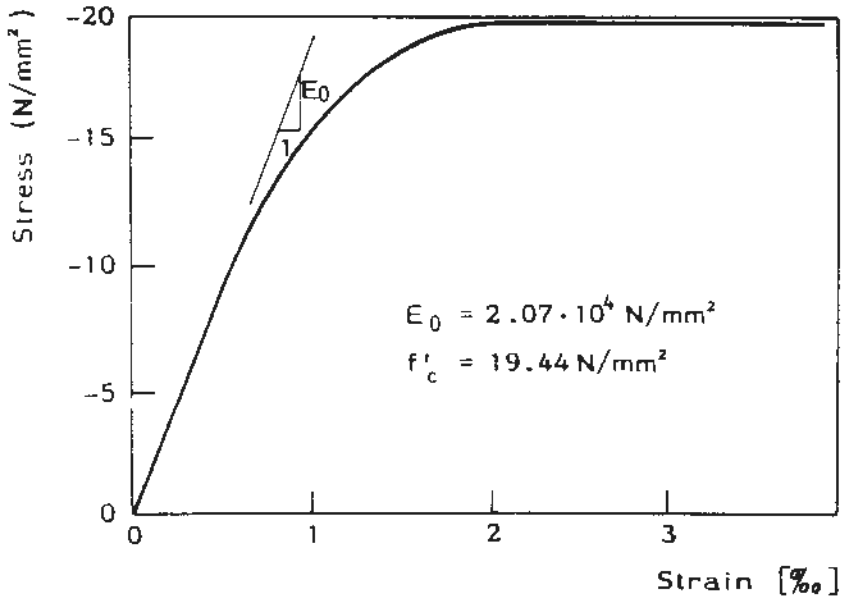

Figure 12 Uniaxial stress-strain curve for concrete.

In Fig. 13 the deflection at midheight as a function of time is shown for the experimental investigations and the present finite element analysis. The creep function at infinity was set equal to $\varphi(\infty,\tau) = 2.30$ and two alternative values were used for $t_{0.5}$, $t_{0.5} = 15$ days and $t_{0.5}$

=30 days. The present investigations showed that the choice of the creep parameters $t_{0.5}$ and $\varphi(\infty,\tau)$ were very decisive for the results.

Unfortunately exact values of $t_{0.5}$ and $\varphi(\infty,\tau)$ are very difficult to find. In many situations it is advisable to be conservative and use a low $t_{0.5}$ and high $\varphi(\infty,\tau)$. The uncertainty of the available data for $t_{0.5}$ and $\varphi(\infty,\tau)$ makes a good case for use of such a simple model as RCM.

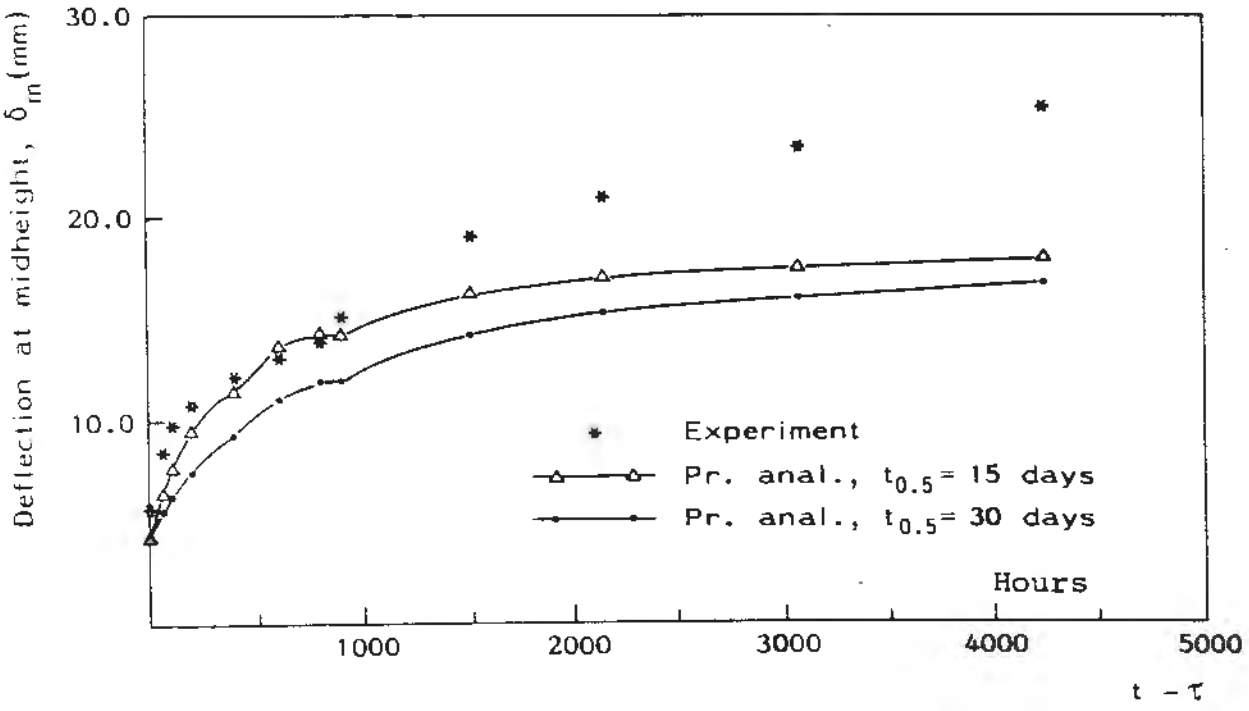

Figure 13 Midspan deflection-time curves. $\varphi(\infty,\tau)$ = 2.30 and $t_{0.5}$ = 15 and 30 days.

The difference is very distinct for the period 1350 hours (56 days) to 4320 hours (180 days). The present analyses show that it is difficult to obtain correct creep behaviour for every period of the first half year (4320 hours) with the rate of creep method.

For all investigations and independent of the time the two most strained integration points over the height are cracked.

The curve that can be drawn through the experimental points in Fig. 13 has not a hyperbolic form as the used creep factor. Observations the latest years /16/ confirm this discrepancy for τ less than 28 days. For higher values of τ the experimental creep factor is more and more coinciding with the theoretical creep factor used in the present investigation.

Calculated creep strains for a period up to 3 months (2160 hours) are mainly sensitive for wrong value of $t_{0.5}$, while after 3 months the creep strains are mainly sensitive for the value of $\varphi(\infty,\tau)$.

9. CONCLUSIONS

Except for A.C.T.Chen and W.F.Chen not much experience has previously been gained with their flow theory for large structures. However, the present study shows that the theory is

well suited for numerical implementation in the membrane elements. The greatest weakness of the theory is the assumptions concerning to the coupling between the equivalent stress-strain in tension and compression. Likewise the strain criteria presented by A.C.T.Chen and W.F. Chen in which straining in the opposite direction as loaded is neglected. Preliminary investigations gave most correct results when the shear retention factor, β, was set equal to 1.0. And therefore this value was always used for the investigations presented here.

According to the combination of flow theories and cracking the principal stresses will drop to a position of pure elastic behaviour after cracking. This case is easy to imagine if cracking in the tension-compression zone. This drastical alternation of the constitutive tensor can give convergence problems. This problem is of course greatest when the crack propagation is high, and when the reinforcement starts yielding. Or more generally, many load steps and many iterations must be used when the determinant of the global stiffness matrix drops essentially. If the tangential stiffness for a given equivalent plastic strain is very low, the accuracy of the strains may be quite low. And this will be transferred to the accuracy of the strains when unloading and reloading. Not only the strains will loose accuracy, but also the displacements. For such problems prescribed displacements should be used instead of prescribed loads.

The accuracy of the creep calculations are also dependent on the steps of the creep factor, which should not be greater than about 10% of the maximum creep factor.

The numerical examples demonstrate the applicability and accuracy of the present approaches. The important factors for failure are in many cases cracking of concrete, yielding of reinforcement, geometric nonlinearities and the size of the load increments. The accuracy of the results obtained indicates that these factors are well represented in the present approach.

10. REFERENCES

1. Bergan, P.G.: "FENRIS-Satellite 1, Theory-Program Outline-Data Input", NTH-SINTEF-VERITEC, Norway 1986
2. Bergan, P.G.: "FENRIS-System, Theory-Program Outline-Data Input", NTH-SINTEF-VERITEC, Norway 1986
3. Chen, A.C.T. and Chen, W.F.: "Constitutive Relations For Concrete", Journal of the Engineering Mechanics Division, Vol. 101, 1975
4. Chen, A.C.T. and Chen, W.F.: "Constitutive Equations and Punch-Indentation of Concrete", Journal of the Engineering Mechanics Division, Vol. 101, 1975
5. Chen, W.F.: "Nonlinear Analysis of Pressure-Resistant Concrete Structures", International Conference on Engineering Application of the Finite Element Method, Vol. 2, Norway 1979
6. Strøm, O.: "Nonlinear Analysis of Reinforced Concrete Structures Using Beam and Membrane Elements", Doctoral Thesis, Report no. 86-1, Div. of Struct. Mech., Norwegian Institute of Technology, Trondheim
7. Chen, W.F.: "Plasticity in Reinforced Concrete", McGraw-Hill Book Company, U.S.A. 1982
8. Sørensen, S.I., Arnesen, A. and Bergan, P.G.: "Nonlinear Finite Element Analysis of Reinforced Concrete using Endochronic Theory", Finite Elements in Nonlinear Mechanics (eds. Bergan, P.G. et al.), Vol. 1, Trondheim 1978.

9. Glanville, W.H.: "Studies in Reinforced Concrete III-Creep or Flow of Concrete under Load", Building Research Technical Paper, No. 12, Dept. of Scientific and Industrial Research, London 1930.

10. Dischinger, F.: "Elastische und Plastische Verformungen bei Eisenbetontragwerke", Der Bauingenieur, Vol. 20, 1939.

11. Dischinger, F.: "Untersuchungen uber die Knicksicherheit, die elastische Verformung und das Kriechen des Betons bei Bogenbrucken", Der Bauingenieur, Vol. 18, 1937.

12. Burns, N.H. and Siess, C.P.: "Repeated and Reversed Loading in Reinforced Concrete". ASCE, Journ. of the Struct. Div., Vol. 92, ST5, Oct. 1966.

13. Arnesen, A.: "Analysis of Reinforced Concrete Shells Considering Material and Geometric Nonlinearities", Report no. 79-1, Division of Structural Mechanics, The Norwegian Institute of Technology, Trondheim 1979

14. Goyal, B.B. and Jackson, N.: "Slender Concrete under Sustained Load", ASCE Proc., Journal of the Structural Division, Vol. 97, No. ST11, Nov. 1971.

15. Åldstedt, E.: "Nonlinear Analysis of Reinforced Concrete Frames", Report No. 75-1, Division of Structural Mechanics, The Norwegian Institute of Technology, Trondheim 1975

16. CEB - Design Manual on Structural Effects of Time-Dependent Behaviour of Concrete, Switzerland 1984.